

See discussions, stats, and author profiles for this publication at: <https://www.researchgate.net/publication/230580521>

TiO₂-Graphene Nanocomposite as High Performace Photocatalysts

ARTICLE *in* THE JOURNAL OF PHYSICAL CHEMISTRY C · DECEMBER 2011

Impact Factor: 4.77 · DOI: 10.1021/jp207515z

CITATIONS

84

READS

374

3 AUTHORS, INCLUDING:



Václav Stengl

Institute of Inorganic Chemistry v.v.i., Husine...

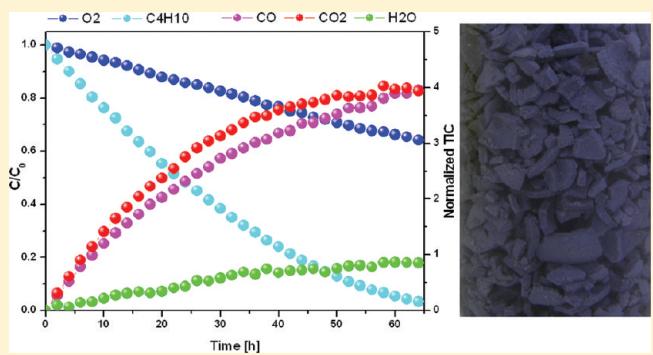
145 PUBLICATIONS 1,764 CITATIONS

SEE PROFILE

TiO₂–Graphene Nanocomposite as High Performance Photocatalysts

Václav Štengl,^{*†} Daniela Popelková,[†] and Petr Vláčil[‡][†]Department of Solid State Chemistry, Institute of Inorganic Chemistry, AS CR v.v.i., 250 68 Řež, Czech Republic[‡]Nanogies Ltd., Řípská 1446/4, 10100 Praha, Czech Republic

ABSTRACT: Nonstoichiometric TiO₂–graphene nanocomposite was prepared by thermal hydrolysis of suspension with graphene nanosheets and titania–peroxy complex. The characterization of graphene nanosheets was provided by using an atomic force microscope (AFM). The prepared samples were characterized by Brunauer–Emmett–Teller (BET) surface area and Barrett–Joiner–Halenda porosity (BJH), X-ray diffraction (XRD), infrared spectroscopy (IR), Raman spectroscopy (RS), and transmission electron microscopy (TEM). UV/vis diffuse reflectance spectroscopy was employed to estimate band gap energies. From the titania/graphene samples, a 300 μm thin layer on a piece of glass 10 × 15 cm was created. The photocatalytic activity of the prepared layers was assessed from the kinetics of the photocatalytic degradation of butane in the gas phase. With regard to the degree of mineralization of butane, the sample labeled TiPC0100 and containing 0.1 g of graphene nanosheets then can be considered as the most active sample.



1. INTRODUCTION

Titanium dioxide (titania) is the most attractive photocatalyst, because it is nontoxic, chemically stable, and relatively cheap. The well-known drawback in the use of anatase in the advanced oxidation photocatalytic process is the recombination of e⁻ and h⁺ pairs. The reported attempts to avoid the recombination of electron–hole pairs is based on the doping of titanium dioxide with noble metals, such as Pt, Au, and Pd.^{1,2} Other options to reduce recombination are, for example, Bi₂S₃/TiO₂, CdS/TiO₂, and In₂S₃/TiO₂ heterojunction photocatalyst.³ Some of the pairings that have been used, for example, titanium dioxide with CdS, with the release of cadmium in solution, cause environmental problems. This method also proved to be less suitable because it is very difficult to determine the correct concentration of the metal. In addition, the interaction between the used metals and disassembly agent (pollutants) reduces photocatalytic efficiency. This problem can be resolved by combining titania and graphene nanosheets.

Graphene is a very attractive material for fabricating graphene containing inorganic composites because of its unique electronic property, high transparency, flexible structure, and large theoretical specific surface area, etc. One of its many applications is the use of graphene in the preparation of highly photoactive composites materials based on titanium oxides.

Graphene is the ideal nanostructure product to be paired with titanium dioxide, increasing its capability to absorb as well as its photocatalytic activity. The electrons freed after the titanium dioxide activation are easily transported to the graphene nanosheets and recombination of e⁻ and h⁺ is strongly reduced, which increases the process yield.

In the literature we can find some efforts to produce these composite materials. A novel method was developed to synthesize

graphite oxide/TiO₂ composites as a highly efficient photocatalyst by in situ depositing TiO₂ nanoparticles on graphene oxide nanosheets by a liquid-phase deposition, followed by a calcination treatment at 200 °C.⁴ New composites of carbon nanosheets and titania nanoparticles with high porosities and high surface area are obtained by simply reassembling exfoliated graphene oxide layers with colloidal titania, in which titania particles with an evident brookite structure or mixed phases of anatase and brookite are encapsulated on the basal plane between the inner surfaces of carbon nanosheets.⁵ The nanocomposites of TiO₂/graphene have been prepared via a facile hydrothermal reaction of graphene oxide and TiO₂ in an ethanol–water solvent. The nanocomposite TiO₂/graphene exhibits much higher photocatalytic activity and stability than pure TiO₂ toward the gas-phase degradation of benzene, a volatile aromatic pollutant in air.⁶ The mixture of titania colloidal suspension in ethanol and graphene oxide sonicated for 30 min produces dispersion of graphene oxide sheets coated with the TiO₂ nanoparticles. The direct interaction between TiO₂ particles and graphene sheets hinders the collapse of exfoliated sheets of graphene.⁷ Graphene oxide/TiO₂ composites were synthesized by using the self-assembly method by using TiCl₃ and graphene oxide as reactants. The concentration of graphene oxide in starting solution played an important role in photoelectronic and photocatalytic performance of graphene oxide/TiO₂ composites.⁸ A novel and facile process is reported for water-phase synthesis of high-quality graphene/TiO₂ composite nanosheets, when TiCl₃ was added to an aqueous dispersion of GO

Received: August 5, 2011

Revised: October 26, 2011

Published: November 16, 2011

Table 1. Samples Composition, Surface Area, Porosity, Crystallite Size, and Cell Parameters of TiO₂–Graphene Nanocomposite

sample	graphene [g]	specific surface area [m ² g ⁻¹]	total pore volume [cm ³ g ⁻¹]	micropore surface area [m ² g ⁻¹]	micropore pore volume [cm ³ g ⁻¹]	cryst size [nm]	cell param <i>a</i> [Å]	cell param <i>c</i> [Å]
TiPC0005	0.005	407.2	2.1202			12.3	3.79157	9.49177
TiPC0010	0.01	217.7	0.3050			32.7	3.79280	9.49448
TiPC0050	0.05	132.5	0.6684	0.53		33.2	3.79298	9.49906
TiPC0100	0.1	153.3	0.5876	1.98	0.00041	33.4	3.79334	9.49884
TiPC0200	0.2	163.1	0.5227	7.65	0.00311	37.5	3.79385	9.49940
TiPC0500	0.5	162.3	0.6002	8.51	0.00305	41.0	3.79499	9.50616

under vigorous stirring in the presence of poly(vinylpyrrolidone) at 95 °C.⁹

In work by Lambert,¹⁰ the synthesis and physiochemical characterization of titanium oxide nanoparticle–graphene oxide and titanium oxide nanoparticle-reduced graphene oxide composites was undertaken. TiO₂–GO materials were prepared via the hydrolysis of TiF₄ at 60 °C for 24 h in the presence of an aqueous dispersion of graphene oxide. TiO₂/graphene composite photocatalysts have been prepared by a simple liquid-phase deposition method using titanium tetrafluoride and electron beam irradiation-pretreated graphene as the raw materials.¹¹ The hybrid of graphite oxide/TiO₂ was prepared through the spontaneous exfoliation of bulky graphite oxide and reorganization with TiO₂ nanoparticles as a solar conversion and hydrogen-generating photocatalyst.¹²

TiO₂–graphene oxide intercalated composite has been successfully prepared at 80 °C with graphite oxide and titanium sulfate Ti(SO₄)₂ as initial reactants. Graphene oxide was first exfoliated by NaOH and formed a single and multilayered graphite oxide mixture that could be defined as graphene oxide, [TiO]²⁺ induced by the hydrolysis of Ti(SO₄)₂ diffused into graphene oxide interlayer by electrostatic attraction.¹³ Zhou et al.¹⁴ prepared graphene titania composites through a one-pot solvothermal reaction by using graphite oxide and tetrabutyl titanate as starting materials. TiO₂ particles with anatase phase and a narrow size distribution were dispersed on the surface of graphene sheets uniformly. A graphene/TiO₂ nanocrystals hybrid has been successfully prepared by directly growing TiO₂ nanocrystals on graphene oxide sheets. The direct growth of the nanocrystals on graphene oxide sheets was achieved by a two-step method, in which TiO₂ was first coated on graphene oxide sheets by hydrolysis and crystallized into anatase nanocrystals by hydrothermal treatment in the second step.¹⁵

In this paper, nonstoichiometric TiO₂–graphene nanocomposite was prepared by thermal hydrolysis of suspension with graphene nanosheets and titania–peroxy complex. Pure graphene nanosheets were produced in large quantity from natural graphite by using high intensity cavitation field in the high-pressure ultrasonic reactor. Graphene sheets, with high specific surface area and unique electronic properties, can be used as a good support for TiO₂ to enhance the photocatalytic activity. The relative photocatalytic activity of the prepared thin layers of titania/graphene nanocomposite in poly(hydroxyethyl methacrylate) was assessed by the photocatalytic decomposition of butane under UV and visible light.

A method developed by us for the nonoxidative preparation of graphene (NOPG) belongs to the area called “top down” approaches, it is the preparation without an oxidation and the subsequent reduction of oxidative residues, as stated in the title of the method. A nonoxidative preparation of a colloidal solution of graphene has been underway for a short time period; it is one pot

method, and as such it is continuous, thus very suitable for industrial use.

2. EXPERIMENTAL SECTION

2.1. Preparation of Graphene Doped Titania Samples. All chemical reagents used in the present experiments were obtained from commercial sources and used without further purification. Titanium oxosulfate TiOSO₄, hydrogen peroxide H₂O₂, ethylene glycol OHCH₂CH₂OH, and ammonium hydroxide NH₄OH were supplied by Sigma-Aldrich. Graphene nanosheets were produced in large quantity from natural graphite (Koh-i-noor Grafite Ltd.) using a high intensity cavitation field in a high-pressure ultrasonic reactor (UIP1000hd, Hielscher Ultrasonics GmbH). Thirty grams of natural graphite in suspension with mixture of 900 mL of distilled water and 100 mL of ethylene glycol was irradiated with intense cavitation field 30 min in high pressure ultrasonic reactor (5 bar). The resulting product was filtered and dried at 200 °C. The quantity of graphene depends on the control of physical conditions during the action of the intensive cavitation field. Controlled physical conditions are the temperature, the pressure inside the reactor and the flow of suspension. Main advantage of this process is the use of high-pressure ultrasonic reactor. The quality of such obtained graphene is much higher in contrast to graphene produced by Hummer's method,¹⁶ where graphite is exfoliated and oxidized by treatment with KMnO₄ and NaNO₃ in concentrated H₂SO₄. The mixture of such a strong oxidizing agent may directly cause defects in the crystal lattice whereas, in the preparation of graphene by intensive cavitation field, the anisotropy of the material is used, which influences the character of the spread of acoustic waves in the material and thus leads to delamination.

Due to control of physical conditions in an ultrasonic reactor and the assumption that the concentration of graphene as a dopant will vary in the range 1–0.001%, the production of graphene could be continual and on an industrial scale. By changing its configuration similarly as described above, the apparatus could produce kilograms of graphene per day.

In the typical procedure, 100 mL of 1.6 M titanium oxosulfate (TiOSO₄) was hydrolyzed by slow addition of ammonium hydroxide solution (10%) under constant stirring at temperature of 0 °C in ice bath. The stirring last until the reaction mixture reaches pH 8.0. The obtained white precipitate was separated by filtration. The consequent depuration of sulfate ions from precipitate with distilled water was confirmed by the BaCl₂. The wet precipitate is mixed with 100 mL of 15% hydrogen peroxide solution, thereby a yellow solution of titania–peroxy complex is obtained.

A well-defined quantity (Table 1) of graphene nanosheets was dispersed using ultrasound in a yellow precursor of titania–peroxy complex and annealed on a heated mantle in a round-bottom flask

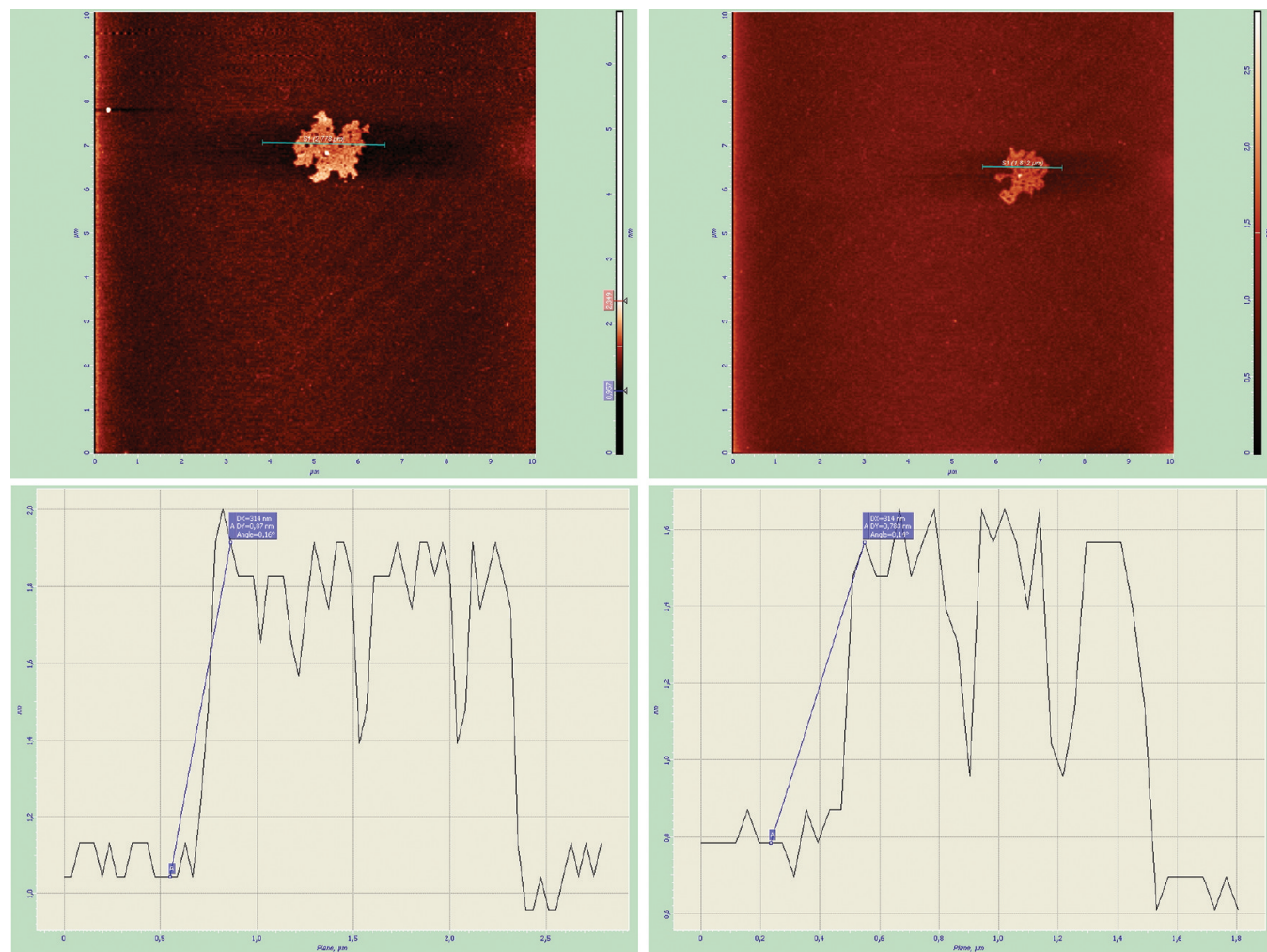


Figure 1. Two independent AFM images of graphene double layers (top) and their profiles (bottom), providing evidencing for the layers being $<0.9\text{ nm}$ thick.

with a reflux cooler at $100\text{ }^{\circ}\text{C}$ for 48 h. The resulting blue titania/graphene nanocomposite was filtered off and dried at $105\text{ }^{\circ}\text{C}$.

The prepared titania/graphene nanocomposite powder (2 g) was dispersed in a mixture of 5 mL of poly(hydroxyethyl methacrylate) and 10 mL of ethanol. From this suspension, a $300\text{ }\mu\text{m}$ thin layer on a piece of glass, $100 \times 150\text{ mm}$, was created.

2.2. Characterization Methods. Diffraction patterns were collected with diffractometer PANalytical X'Pert PRO equipped with conventional X-ray tube ($\text{Cu K}\alpha$ radiation, 40 kV, 30 mA) and a linear position sensitive detector PIXcel with an antiscatter shield. A programmable divergence slit set to a fixed value of 0.5° , Soller slits of 0.02 rad , and mask of 15 mm were used in the primary beam. A programmable antiscatter slit set to a fixed value of 0.5° , Soller slit of 0.02 rad , and $\text{Ni }\beta\text{-filter}$ were used in the diffracted beam. Qualitative analysis was performed with the DiffracPlus Eva software package (Bruker AXS, Germany) using the JCPDS PDF-2 database.¹⁷ For quantitative analysis of XRD patterns we used Difrac-Plus Topas (Bruker AXS, Germany, version 4.1) with structural models based on ICSD database.¹⁸ This program permits us to estimate the weight fractions of crystalline phases and mean coherence length by means of Rietveld refinement procedure.

The morphology of sample powders was inspected by transmission electron microscopy (TEM), and the crystal structure was analyzed by electron diffraction (ED) using a 120 kV TEM microscope Tecnai G2 Spirit (FEI, Czech Republic). As specimen support for TEM investigations, a microscopic copper grid covered with a thin transparent carbon film was used. The samples were studied both in bright field and by electron diffraction with a selecting aperture (SAED) mode at an acceleration voltage of 120 kV.

AFM images were obtained using an NTEGRA Aura (NT-MTD) microscope. A sample of the diluted dispersion was placed on synthetic mica as an atomically smooth support and evaporated at room temperature. The measurements were performed in air at room temperature in noncontact mode, with Si tips of the 1650-00 type at resonance frequencies ranging from 180 to 240 kHz.

The surface areas of samples were determined from nitrogen adsorption-desorption isotherms at liquid nitrogen temperature using a Coulter SA3100 instrument with outgas 15 min at $150\text{ }^{\circ}\text{C}$. The Brunauer–Emmett–Teller (BET) method was used for surface area calculation,¹⁹ and the pore size distribution (pore diameter, pore volume, and micropore surface area of the samples) was determined by the Barrett–Joyner–Halenda (BJH) method.²⁰

The Raman spectra were acquired with DXR Raman microscope (Thermo Scientific) with a 532 nm (6 mW) laser, 32 2-s scans were accumulated with laser 532 nm (6 mW) under 10 \times objective of Olympus microscope.

Infrared spectra were recorded by using a Thermo-Nicolet Nexus 670 FT-IR spectrometer approximately in 4000–500 and 500–50 cm^{-1} , respectively, with a single-reflection horizontal accessory on Si crystal. The samples were mixed with KBr and pressed to conventional pellets at ambient conditions and measured in the transmission mode.

Diffuse reflectance UV/vis spectra for evaluation of photochemical properties were recorded in the diffuse reflectance mode (R) and transformed to absorption spectra through the Kubelka–Munk function.²¹ A Perkin-Elmer Lambda 35 spectrometer equipped with a Labsphere RSAPE- 20 integration sphere with BaSO_4 as a standard was used. The reflectance data were obtained as a relative percentage reflectance to a nonabsorbing material (BaSO_4), which can optically diffuse light.

Kinetics of the photocatalytic degradation of butane was measured using a homemade stainless steel batch photoreactor²² with a Narva black-light fluorescent lamp at wavelength 365 nm and warm-white fluorescent lamp at wavelength up to 400 nm (input power 8 W, light intensity 6.3 mW cm^{-2}). The gas concentration was measured by a quadrupole mass spectrometer JEOL JMS-Q100GC and gas chromatograph Agilent 6890N. A high-resolution gas chromatography column (19091P-QO4, J&W Scientific) was used. Samples were taken from the reactor automatically through the sampling valve (six-port external volume sample injector VICI, Valco Instruments Co. Inc.) in a time interval of 2 h.

Blank tests (a layer of poly(hydroxyethyl methacrylate) without titania) were performed to establish the effect of photolysis and catalysis on the conversion of butane. The UV irradiation detects that there was no or immeasurable conversion of butane, as a testing gas, into CO and/or CO_2 , and consequently butane also did not absorb on the poly(hydroxyethyl methacrylate) matrix. The injection volume of butane into the photoreactor was 30 mL.

3. RESULTS AND DISCUSSION

The quality of graphene prepared by NOPG is higher than that for the graphene obtained by reducing of the oxide graphite (e.g., Hummer's method).¹⁶ Due to strong oxidation agents, oxidative preparation of graphene can cause defects on the released π bonds or defects directly in the crystal lattice of the graphene. These defects can cause nonstandard behavior in the interaction of graphene/element, which causes difficulties in the preparation of chemical mixtures. In Figure 1 the characteristic image from AFM microscopy of prepared graphene nanosheets can be seen.

The thermal hydrolysis of the titania–peroxy complex leads to spindle-like particles. The direct interaction between TiO_2 nanoparticles and graphene sheet prevents the reaggregation of the exfoliated sheets of graphene. The origin of the blue coloration is from the Ti^{3+} ions. The intensity of blue coloration increases along with amount of graphene. Thanks to the presence of H_2O_2 , graphene nanosheets are in part oxidized to graphene oxide nanosheets and Ti^{3+} ion is formed. Digital images of the as-synthesized samples are shown in Figure 2. Figure 2a was taken from the pure graphene powder; Figure 2b is the yellow titania–peroxy complex gel. As shown in Figure 2c, after refluxing for

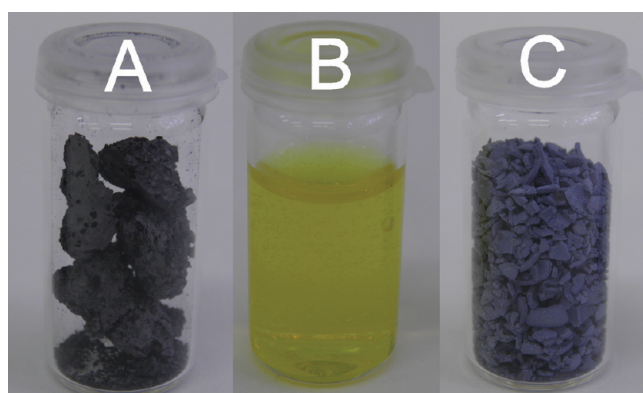


Figure 2. (a) Pure graphene powder, (b) yellow titania peroxo complex gel, and (c) titania–graphene nanocomposite.

48 h, the color of the mixture solution turns from yellow to blue. The origin of the blue coloration is from the Ti^{3+} ions.²³

Figure 3 shows X-ray diffraction patterns of titania/graphene nanocomposites. All samples show the major phase of anatase (PDF 21-1272) with a small amount of the brookite phase (see peak labeled B121, PDF 29-1360). Nevertheless, the intensities of brookite X-ray lines are too low for performing Rietveld refinement with good quality. The graphene showed a peak at $2\Theta = 26.50^\circ$ (see arrow G),^{24,25} which increased in intensity with the amount of graphene in the nanocomposite. Crystallite size, a and c cell parameters of anatase, calculated by the Rietveld refinement procedure using the Topas v.4.2 program, are listed in Table 1. The increase of lattice parameters a and c for the titania/graphene nanocomposite is expected to occur if some of the Ti^{4+} are transformed to Ti^{3+} , because of the larger ionic radius of Ti^{3+} (0.670 Å) compared to Ti^{4+} (0.605 Å).²⁶ A growing amount of graphene and the concentration of Ti^{3+} ions is accompanied by a bluer color of samples.

The specific surface area of the prepared titania/graphene nanocomposites calculated by the multipoint Brunauer–Emmett–Teller (BET) method, total pore volume, micropore surface area, and micropore volume are listed in Table 1. The Barrett–Joyner–Halenda (BJH) pore-size distribution plot and nitrogen adsorption/desorption isotherms are shown in Figure 4. According to IUPAC notation,²⁷ microporous materials have pore diameters smaller than 2 nm and macroporous materials have pore diameters greater than 50 nm; the mesoporous category thus lies in the middle. As for all the titania/graphene nanocomposites, the isotherm form corresponds to that of type IV isotherm classification and the type E hysteresis loop is in agreement with the De Boer classification attributed to mesoporous solids.²⁸ The average pore size lies between 10 and 25 nm. Along with the decreasing content of the graphene nanosheet, the pore size distribution of TiO_2 /graphene nanocrystals are relatively narrow respectively. An increasing of graphene nanosheets in the nanocomposite content leads to a decrease of specific surface area and also to a slight increase in formation of microporous texture (Table 1). The origin of microporous texture can negatively reflect in the lower photocatalytic activity.

Figure 5a,b shows low magnification and high resolution TEM images of prepared graphene nanosheets. Graphene nanosheets tend to congregate together to form multilayer agglomerates. As shown in Figure 5b, HRTEM images clearly illustrate the crystalline nature of the graphene nanosheet. The FFT was used to calculate graphene layer spacing in its crystalline lattice. The FFT

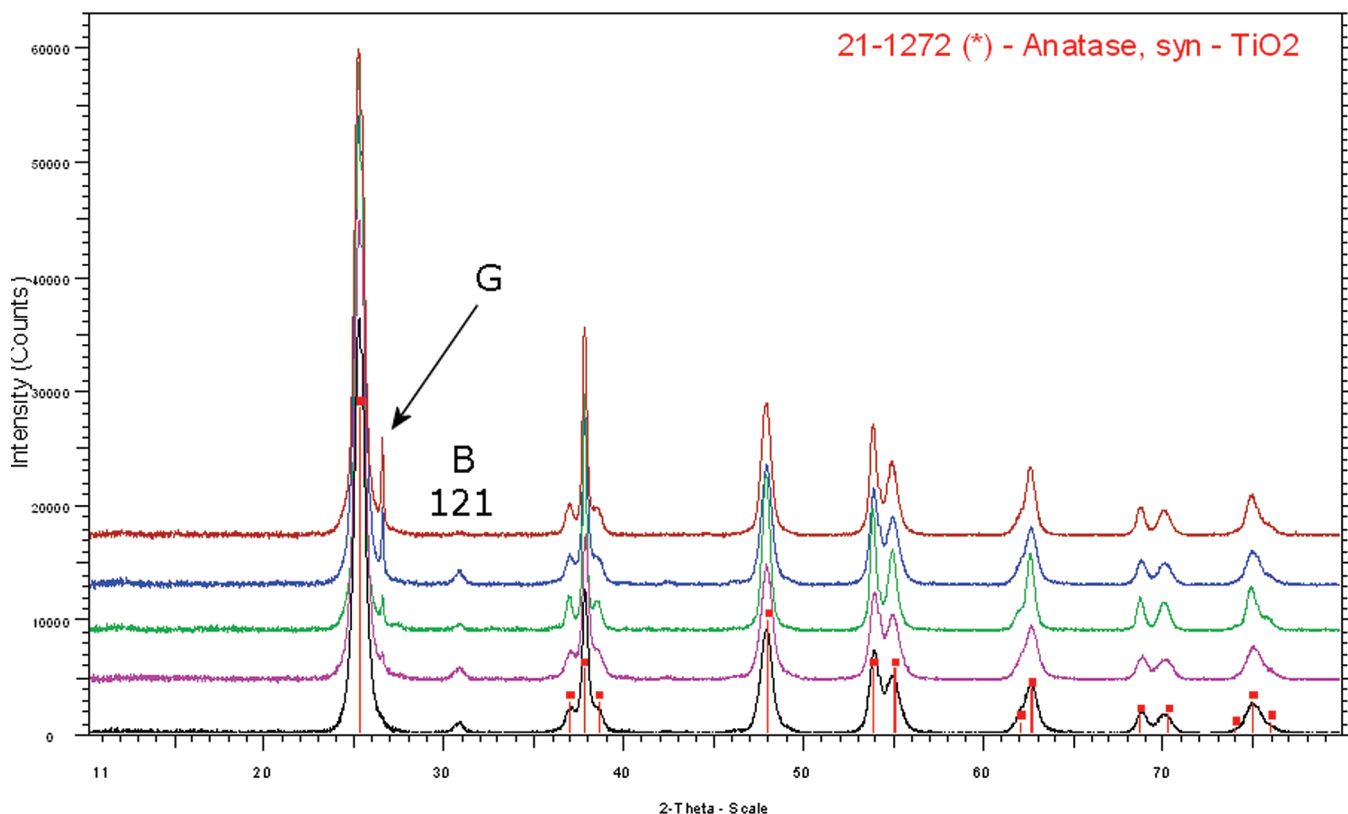


Figure 3. XRD patterns of titania–graphene nanocomposite (G, graphene; B121, brookite).

answer in graphene prepared by our “top-down” method is 0.32 nm. In the ideal graphite, crystalline layer spacing would be expected to be 0.34 nm. Due to releasing intercrystalline-layer π bonds, lattice layer spacing is slightly smaller.²⁹ The spindle-like TiO_2 particles are a product of the titania–peroxy complex thermal hydrolysis.³⁰ Graphene nanosheets are prevented from reaggregation by direct interaction in between TiO_2 and graphene nanosheets themselves (see arrows, Figure 5c,d). Selected area electron diffraction (SAED) was performed on the graphene nanosheets and TiO_2 /graphene composite and the corresponding SAED image is shown as the inset in Figure 5a,c.

The Raman spectra of titania/graphene nanocomposites are presented in Figure 6. The specific vibration modes are located around 143 cm^{-1} (E_g), 395 cm^{-1} (B_{1g}), 513 cm^{-1} ($B_{1g} + A_{1g}$), and 634 cm^{-1} (E_g), indicating the presence of the anatase phase in all of these samples. The measured frequencies of peak positions vary among the samples; with increasing content of graphene particles (or content of Ti^{3+} ions) at low frequency, the E_g mode shifts from 143.3 to 148.4 cm^{-1} (Table 2). The measured values of Raman spectra are in good agreement with values for anatase, as well as nonstoichiometric titanium oxide containing Ti^{3+} .³¹ The Raman shifts may be also affected by the growing anatase crystallite size, as is evident from Table 1.³²

Figure 7 shows the IR spectrum of the titania/graphene nanocomposite prepared by thermal hydrolysis of titania–peroxy complexes. The broad absorption peaks about 3400 cm^{-1} , and the band at 1635 cm^{-1} corresponds to the surface absorbed water and the hydroxyl groups.³³ The band at 650 cm^{-1} is most probably related to the $\text{Ti}–\text{O}$ vibration modes of the $\text{Ti}^{3+}–\text{O}–\text{Ti}^{4+}$ framework.³⁴ Surface adsorbed sulfate ions can probably be assigned to a band at 1100 cm^{-1} .³⁵

Figure 8a presents UV-vis absorption spectra of the as-prepared samples of the titania/graphene nanocomposite. The reflectance data obtained were a relative percentage reflectance to a nonabsorbing material (BaSO_4) that can optically diffuse light. The Kubelka–Munk theory is generally used for the analysis of diffuse reflectance spectra obtained from weakly absorbing samples.³⁶ Compared with the pure titania sample (TiPC000), for the titania/graphene nanocomposite obvious absorption edge red shifts are observed in the results, among which the best response to visible light is obtained in these samples with the content of Ti^{3+} ions. With increasing graphene content, the prepared samples are beginning to have a light blue color; the sample marked TiPC05 containing 0.5 g of graphene is dark blue. Pure titania powder can absorb only light with wavelengths smaller than 400 nm, whereas for the titania/graphene nanocomposite with Ti^{3+} ions, the light absorption extends to the visible-light region.

The method of UV-vis diffuse reflectance spectroscopy was employed to estimate band gap energies of the prepared titania/graphene nanocomposites. First, to establish the type of band-to-band transition in these synthesized particles, the absorption data were fitted to equations for direct band gap transitions.³⁷ Figure 8b shows the $(\alpha h\nu)^2$ versus photon energy $h\nu$ for a direct band gap transition. The resulting extrapolated values of E_{bg} for the direct transitions are listed in Table 3. The value of 3.20 eV for reference sample denoted as TiPC000 is reported in the literature for pure anatase nanoparticles.^{38,39} The value of band gap energy decreases with an increasing content of the graphene dopant and increasing content of Ti^{3+} ions.

The graphene nanosheet has a dual task in the nanocomposite. First, it makes Ti^{3+} ions stable in the TiO_2 matrix, and second, it forms a heterojunction system with titania. Graphene works as a

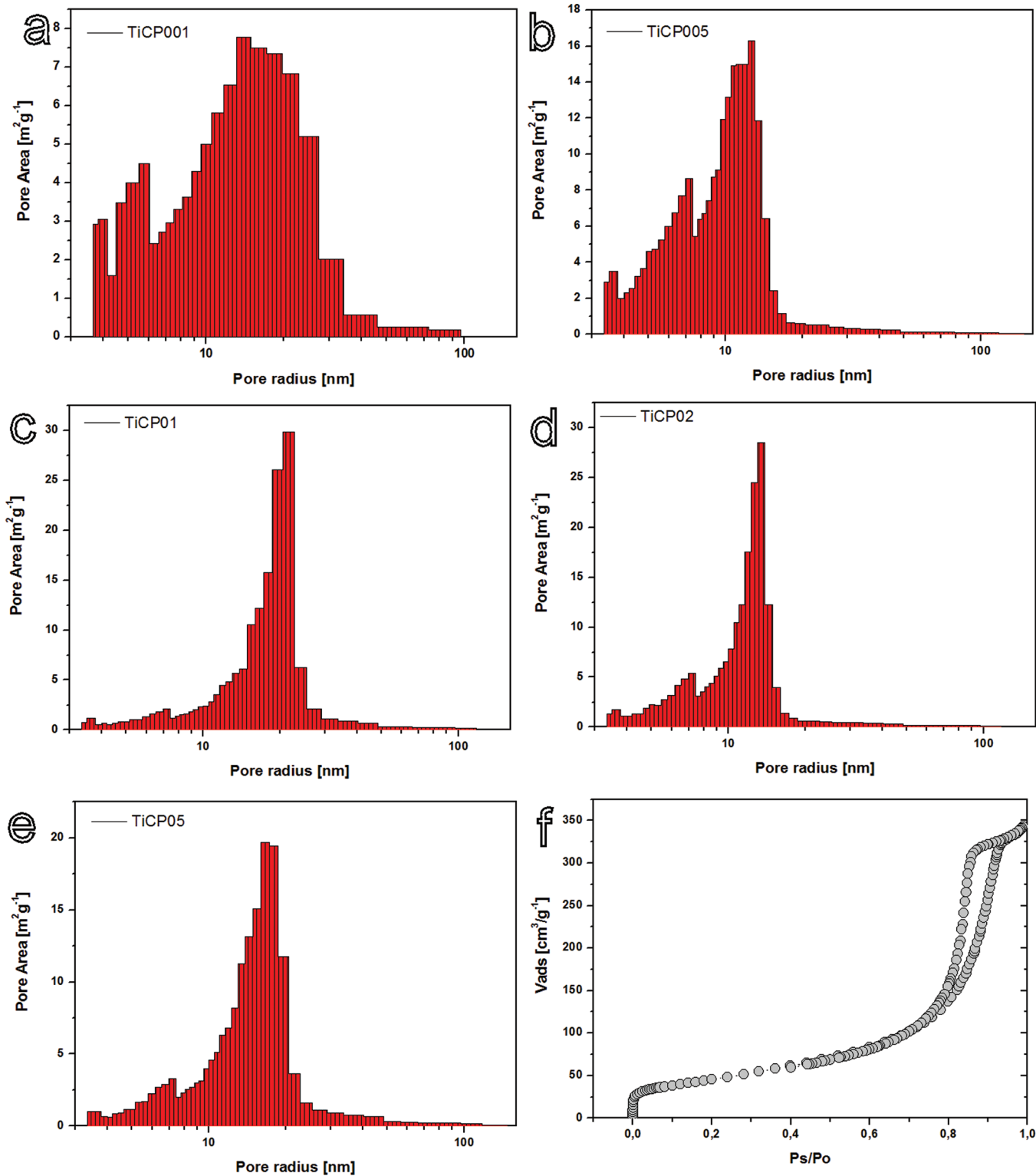


Figure 4. Pore surface area and adsorption–desorption isotherms of samples: (a) TiPC0010; (b) TiPC0050; (c) TiPC0100; (d) TiPC0200; (e) TiPC0500; (f) hysteresis loop.

sensitizer, and TiO_2 works as a substrate in the heterojunction system. Under UV and visible light irradiation, photoinduced electrons on the titania surface can easily transfer to graphene nanosheets and, analogously, photoinduced holes on the graphene nanosheets surface would migrate into titania. In this way, the photoinduced electron–hole pairs in the catalyst, are effectively

separated and the probability of electron–hole recombination is reduced. The Ti^{3+} state in the TiO_2 lattice originate from non-stoichiometry, oxygen deficiency, and ion intercalation, as well as surface adsorbed species and other surface or interface states. Ti^{3+} surface states of TiO_2 act as a photocatalytic active site and the increase of the photocatalytic activity of TiO_2 is due to the increase

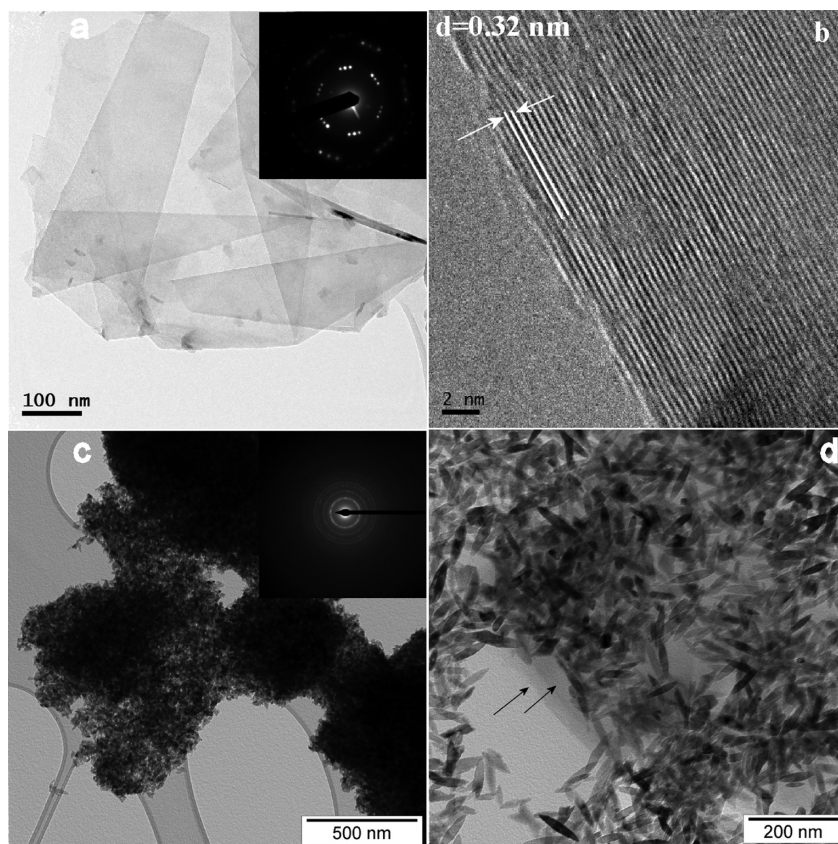


Figure 5. (a) TEM images of graphene, (b) HRTEM images of graphene, and (c, d) TEM images of graphene–titania nanocomposite.

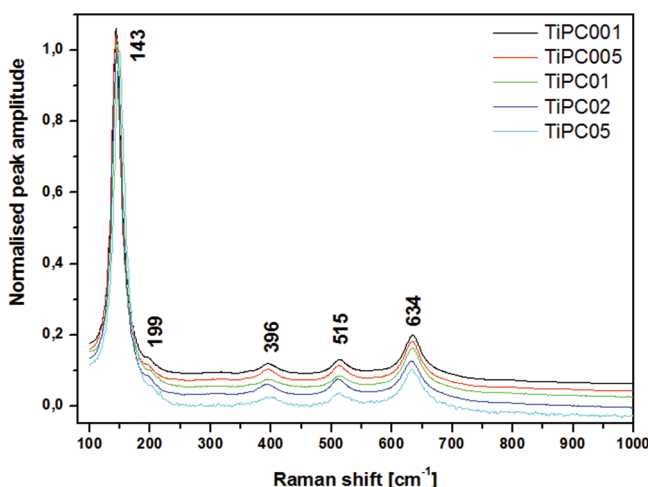


Figure 6. Raman spectra of graphene–titania nanocomposite.

of Ti^{3+} concentration, occurring as a result of the titania ion valence change from Ti^{4+} to Ti^{3+} .

The photocatalytic activity of the prepared layers of titania/graphene samples was assessed from the kinetics of the photocatalytic degradation of butane in the oxygen atmosphere. Photocatalytic oxidation of butane is based on the following overall reactions:⁴⁰



Figure 9 shows the typical chromatograph of the effluent obtained near butane photocatalytic degradation. Only oxygen,

Table 2. Raman Shifts [cm^{-1}] of TiO_2 –Graphene Nanocomposite

sample	E_g	B_{1g}	$B_{1g} + A_{1g}$	E_g
TiPC0010	143.3	395.1	513.6	634.1
TiPC0050	143.3	395.9	512.6	633.1
TiPC0100	145.3	395.1	512.6	634.1
TiPC0200	144.3	395.1	512.6	632.2
TiPC0500	148.4	400.1	513.8	632.4

carbon monoxide, carbon dioxide, water and butane were detected at retention times of 1.52, 1.54, 2.41, 6.42, and 9.53 min. Besides the kinetics of starting components (butane and molecular oxygen), there were monitored time profiles of photocatalytic products (carbon dioxide, carbon monoxide, and water) as well.

The typical corresponding experimental dependencies in time are plotted in Figure 10. The rate of degradation was estimated to obey pseudo-first-order kinetics, and hence the rate constant for degradation k was obtained from the first-order plot according to eq 2, where c_0 is the initial concentration, c is the concentration of butane after time (t), and k is the first-order rate constant:

$$\ln(c/c_0) = kt \quad (2)$$

The photocatalytic degradation of butane was fitted by curves of the first-order kinetics and the corresponding rate constants are given in Table 3. Djeghri et al.⁴¹ reported photoinduced oxidation of C2–C8 alkanes on TiO_2 at ambient temperature.

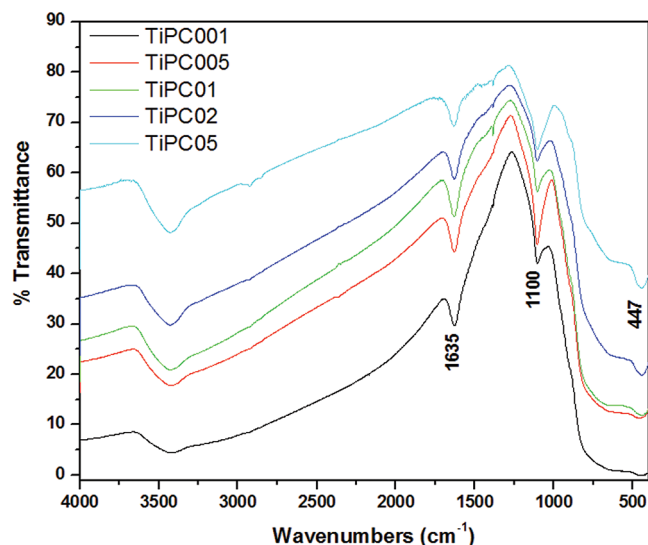


Figure 7. Infrared spectra of graphene–titania nanocomposite.

In general, they observed that alkanes (C_nH_{2n+2}) formed ketones ($C_nH_{2n}O$) and other aldehydes $C_mH_{2m}O$ with $2 < m < n$. If the alkane was branched, the ketone was $C_mH_{2m}O$ with $3 < m < n$. The reactivity of different types of carbon atoms followed the sequence: $C_{\text{tertiary}} > C_{\text{quaternary}} > C_{\text{secondary}} > C_{\text{primary}}$. Figure 9 shows that, in our case, the reactivity of butane is different and simpler—no intermediate products such as lower alkane or ketone were detected in the gaseous phase. This means that photocatalytic oxidation proceeds not in the gaseous phase but only on the layer surface directly, causing formation of CO, CO_2 , and H_2O .

Before each measurement, the reactor is first evacuated and then rinsed with the O_2 . If the measured gas chromatogram shows only the oxygen peak at retention time 1.52 min, then a gas for the photocatalytic decomposition (in our case the butane) can be injected. After the subsequent chromatogram is measured, peaks for the O_2 and the butane are each marked by a value of 1. The values of gases, which are expected to be formed due to photoactivity of the composite $\text{TiO}_2/\text{graphene}$ (CO, CO_2), are each assigned a value of 0. By this, input data are normalized and the measurement with time period 2 h can be started.

The normalized total ion current (TIC) for CO, CO_2 , and H_2O after time reaction 60 h is presented in Table 3.

The measured results show that the photocatalytic decomposition of butane in the UV and visible light the sample labeled TiPC010 has the highest photocatalytic activity. An increasing content of graphene, however, lowers the rate of photodegradation of butane and marked increase of carbon monoxide and carbon dioxide. This suggests that in these samples there is a much deeper mineralization at the expense of the primary decomposition of butane. Increased content of Ti^{3+} can enhance the photocatalytic performance of TiO_2 , because the exterior energy of Ti^{3+} is 0.3 eV lower than the conductive band of TiO_2 and thereby creates a trap for electrons generated by the light and limits the recombination of electrons and holes.⁴² The highest increase of CO and CO_2 is in sample TiPC0100 containing 0.01 g of graphene nanosheets.

Furthermore, the photoexcited electrons and holes in the lattice are separated and trapped by appropriate sites of TiO_2 to avoid recombination. The interaction of CO_2 molecules with the

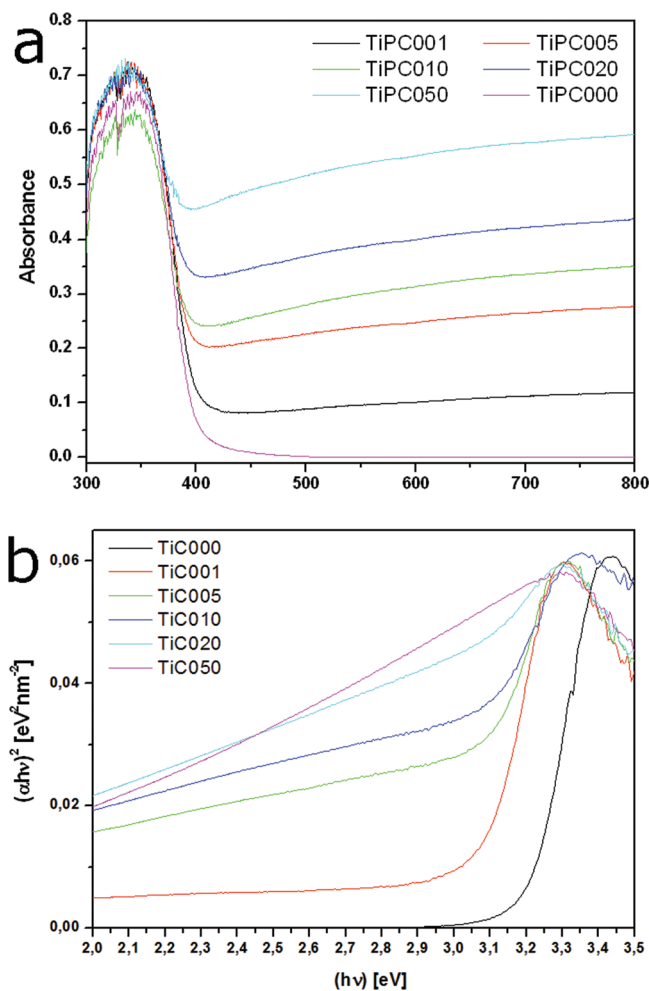


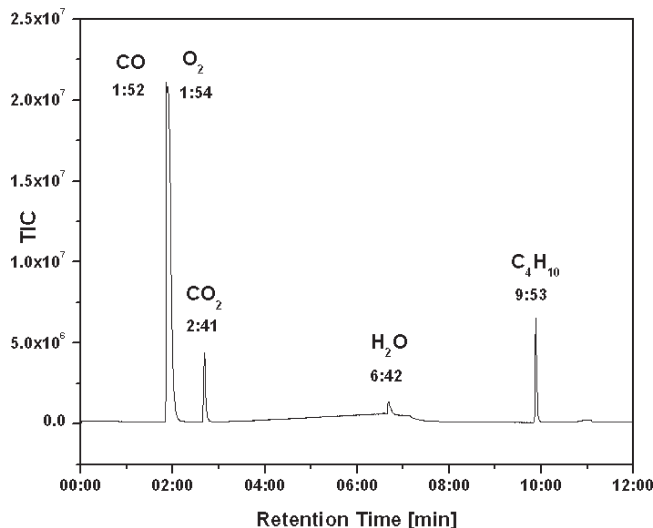
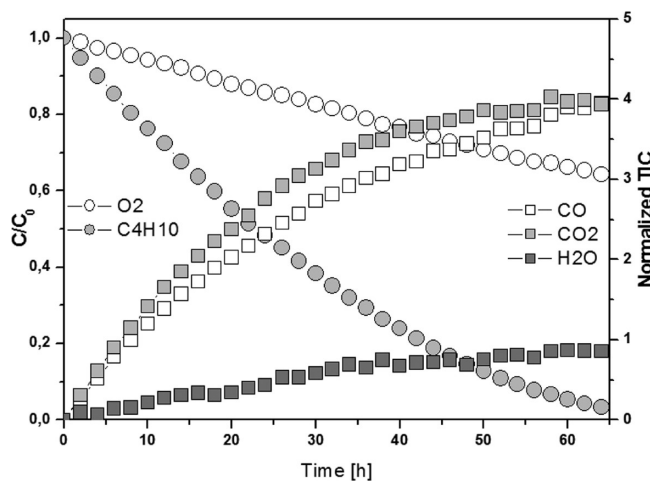
Figure 8. (a) UV–vis diffuse absorbance spectra. (b) Band-gap energy of graphene–titania nanocomposite.

excited state of Ti^{3+} — O^- leads to the formation of $\text{CO}_2^{\bullet-}$ anion radicals. $\text{CO}_2^{\bullet-}$ anion radicals formed in solvents of high dielectric constant (water) results in weak interaction of the radical with the photocatalyst surface and leads to the formation of formic acid instead of carbon monoxide. However, solvents with lower dielectric constant (poly(hydroxyethyl metacrylate)) readily lead to the formation of carbon monoxide due to its strong adsorption on Ti sites of the TiO_2 surface.⁴³ From the results²² we found that titania prepared with anionic surfactant has a three times better (higher) photocatalytic activity at photocatalytic degradation butane than titania prepared with cationic surfactant. These mesoporous materials free of Ti^{3+} ions at photocatalytic decomposition of butane at UV and visible light have higher amount of CO_2 than CO. In contrast, the titania/graphene composites containing Ti^{3+} ions and on the other hand they have higher amount of CO than CO_2 . With regard to the degree of mineralization of butane it can then be considered as the most active sample labeled TiPC0100 containing 0.1 g of graphene nanosheets.

In the case of titania–graphene nanocomposites, a heterojunction forms at the interface, where there is a space–charge separation region. Electrons have a tendency to flow from the higher to lower Fermi level to adjust the Fermi energy levels.⁴⁴ The calculated work function of graphene is 4.42 eV and the

Table 3. Band-Gap Energy, Rate Constant k , and TIC for CO, CO₂, and H₂O of TiO₂–Graphene

sample	E _{bg} [eV]	$k(365 \text{ nm}) [\text{h}^{-1}]$	CO [TIC]	CO ₂ [TIC]	H ₂ O [TIC]	$k(400 \text{ nm}) [\text{h}^{-1}]$	CO [TIC]	CO ₂ [TIC]	H ₂ O [TIC]
TiPC0000	3.20	0.02686	4	7	2	0.00959	7	8	2
TiPC0005	3.10	0.01350	10	18	4	0.00911	4	6	2
TiPC0010	3.05	0.03689	4	4	1	0.01317	5	7	1
TiPC0050	2.90	0.01357	4	15	4	0.00770	6	10	3
TiPC0100	2.70	0.01991	58	28	27	0.00530	36	15	3
TiPC0200	2.40	0.01245	6	20	3	0.00360	8	9	2
TiPC0500	>2	0.01004	11	34	3	0.00527	5	5	2

**Figure 9.** Gas chromatograph of butane.**Figure 10.** Kinetics of the photocatalytic degradation of butane on layer of sample TiPC0010.

conduction band position of anatase is about -4.21 eV with a band gap of about 3.2 eV , graphene can accept the photoexcited electrons from TiO₂.¹⁴ In this way, the photoinduced electron–hole pairs are effectively separated and the probability of electron–hole recombination is reduced. In the titania–graphene nanocomposites the highest photocatalytic mineralization for UV and visible light was observed by the sample denoted TiPC0100, which has probably the optimum ratio of titania: graphene. With

increasing content of graphene, there are too many graphene nanosheets on the titania surface, which hinders the contact of TiO₂ with butane, resulting in too many electrons accumulating on the TiO₂ surface under light irradiation, leading to lower photocatalytic activity.

4. CONCLUSION

Nonstoichiometric TiO₂–graphene nanocomposite was prepared by one-pot thermal hydrolysis of suspension graphene nanosheets and titania peroxy complex as starting materials. Graphene nanosheets were produced in large quantity from natural graphite using a high intensity cavitation field in high-pressure ultrasonic reactor.

The direct interaction between TiO₂ nanoparticles and graphene sheet prevents the reaggregation of the exfoliated sheets of graphene. In the presence of hydrogen peroxide, the graphene nanosheets are partially oxidized to graphene oxide nanosheets and Ti³⁺ ion forms. The graphene nanosheets make Ti³⁺ ions stable in the TiO₂ matrix and form a heterojunction system with titania. The best photocatalytic mineralization of titania–graphene nanocomposites is highest under UV and visible light and is for the sample denoted TiPC0100 with an optimum ratio of titania and graphene.

■ AUTHOR INFORMATION

Corresponding Author

*E-mail: stengl@iic.cas.cz. Tel.: 420 2 6617 2193. Fax: 420 2 2094 0157.

■ ACKNOWLEDGMENT

The work was supported by Ministry of Industry and Trade of the Czech Republic Project No. FI-IM3/061 and FI-IM5/239. We gratefully thank K. Safářová (Regional Centre of Advanced Technologies and Materials, Faculty of Science, Palacký University in Olomouc) for AFM measurement.

■ REFERENCES

- (1) Kim, S.; Hwang, S. J.; Choi, W. Y. Visible light active platinum-ion-doped TiO₂ photocatalyst. *J. Phys. Chem. B* **2005**, *109* (51), 24260–24267.
- (2) Sobana, N.; Muruganadham, M.; Swaminathan, M. Nano-Ag particles doped TiO₂ for efficient photodegradation of Direct azo dyes. *J. Mol. Catal. A: Chem.* **2006**, *258* (1–2), 124–132.
- (3) Bessekhouad, Y.; Robert, D.; Weber, J. V. Bi₂S₃/TiO₂ and CdS/TiO₂ heterojunctions as an available configuration for photocatalytic degradation of organic pollutant. *J. Photochem. Photobiol., A* **2004**, *163* (3), 569–580.
- (4) Jiang, G. D.; Lin, Z. F.; Chen, C.; Zhu, L. H.; Chang, Q.; Wang, N.; Wei, W.; Tang, H. Q. TiO₂ nanoparticles assembled on graphene

- oxide nanosheets with high photocatalytic activity for removal of pollutants. *Carbon* **2011**, *49* (8), 2693–2701.
- (5) Liu, Y. J.; Wang, Z. M.; Aizawa, M.; Peng, W. Q.; Hirotsu, T. Nanoporous composite of carbon nanosheets and functional titania nanoparticles formed by reassembling of exfoliated graphite oxides with colloidal titania. *Mater. Lett.* **2009**, *63* (2), 260–262.
- (6) Zhang, Y. H.; Tang, Z. R.; Fu, X. Z.; Xu, Y. J. TiO₂-Graphene Nanocomposites for Gas-Phase Photocatalytic Degradation of Volatile Aromatic Pollutant: Is TiO₂-Graphene Truly Different from Other TiO₂-Carbon Composite Materials? *ACS Nano* **2010**, *4* (12), 7303–7314.
- (7) Williams, G.; Seger, B.; Kamat, P. V. TiO₂-graphene nanocomposites. UV-assisted photocatalytic reduction of graphene oxide. *ACS Nano* **2008**, *2* (7), 1487–1491.
- (8) Chen, C.; Cai, W. M.; Long, M. C.; Zhou, B. X.; Wu, Y. H.; Wu, D. Y.; Feng, Y. J. Synthesis of Visible-Light Responsive Graphene Oxide/TiO₂ Composites with p/n Heterojunction. *ACS Nano* **2010**, *4* (11), 6425–6432.
- (9) Zhu, C. Z.; Guo, S. J.; Wang, P.; Xing, L.; Fang, Y. X.; Zhai, Y. M.; Dong, S. J. One-pot, water-phase approach to high-quality graphene/TiO₂ composite nanosheets. *Chem. Commun.* **2010**, *46* (38), 7148–7150.
- (10) Lambert, T. N.; Chavez, C. A.; Hernandez-Sanchez, B.; Lu, P.; Bell, N. S.; Ambrosini, A.; Friedman, T.; Boyle, T. J.; Wheeler, D. R.; Huber, D. L. Synthesis and Characterization of Titania-Graphene Nanocomposites. *J. Phys. Chem. C* **2009**, *113* (46), 19812–19823.
- (11) Zhang, H. J.; Xu, P. P.; Du, G. D.; Chen, Z. W.; Oh, K.; Pan, D. Y.; Jiao, Z. A facile one-step synthesis of TiO₂/graphene composites for photodegradation of methyl orange. *Nano Res.* **2011**, *4* (3), 274–283.
- (12) Park, Y.; Kang, S. H.; Choi, W. Exfoliated and reorganized graphite oxide on titania nanoparticles as an auxiliary co-catalyst for photocatalytic solar conversion. *Phys. Chem. Chem. Phys.* **2011**, *13* (20), 9425–9431.
- (13) Zhang, Q. O.; He, Y. Q.; Chen, X. G.; Hu, D. H.; Li, L. J.; Yin, T.; Ji, L. L. Structure and photocatalytic properties of TiO₂-Graphene Oxide intercalated composite. *Chin. Sci. Bull.* **2011**, *56* (3), 331–339.
- (14) Zhou, K. F.; Zhu, Y. H.; Yang, X. L.; Jiang, X.; Li, C. Z. Preparation of graphene-TiO₂ composites with enhanced photocatalytic activity. *New J. Chem.* **2011**, *35* (2), 353–359.
- (15) Liang, Y. Y.; Wang, H. L.; Casalongue, H. S.; Chen, Z.; Dai, H. J. TiO₂ Nanocrystals Grown on Graphene as Advanced Photocatalytic Hybrid Materials. *Nano Res.* **2010**, *3* (10), 701–705.
- (16) Hummers, W. S.; Offeman, R. E. Preparation of graphitic oxide. *J. Am. Chem. Soc.* **1958**, *80* (6), 1339–1339.
- (17) JCPDS, PDF 2 database, Release 50, International Centre for Diffraction Data, Newtown Square, 2000.
- (18) ICSD, ICSD Database, FIZ Karlsruhe, Germany, 2008.
- (19) Brunauer, S.; Emmett, P. H.; Teller, E. Adsorption of gases in multimolecular layers. *J. Am. Chem. Soc.* **1938**, *60*, 309–319.
- (20) Barrett, E. P.; Joyner, L. G.; Halenda, P. P. The determination of pore volume and area distributions in porous substances 0.1. Computations from nitrogen isotherms. *J. Am. Chem. Soc.* **1951**, *73* (1), 373–380.
- (21) Orel, Z. C.; Gunde, M. K.; Orel, B. Application of the Kubelka-Munk theory for the determination of the optical properties of solar absorbing paints. *Prog. Org. Coat.* **1997**, *30* (1–2), 59–66.
- (22) Stengl, V.; Houskova, V.; Bakardjieva, S.; Murafa, N.; Havlin, V. Optically Transparent Titanium Dioxide Particles Incorporated in Poly(hydroxyethyl methacrylate) Thin Layers. *J. Phys. Chem. C* **2008**, *112* (50), 19979–19985.
- (23) Ookubo, A.; Kanezaki, E.; Ooi, K. ESR, XRD, and DRS studies of paramagnetic Ti³⁺ ions in a colloidal solid of titanium-oxide prepared by the hydrolysis of TiCl₃. *Langmuir* **1990**, *6* (1), 206–209.
- (24) Saner, B.; Okyay, F.; Yurum, Y. Utilization of multiple graphene layers in fuel cells. 1. An improved technique for the exfoliation of graphene-based nanosheets from graphite. *Fuel* **2010**, *89* (8), 1903–1910.
- (25) Wang, G. X.; Yang, J.; Park, J.; Gou, X. L.; Wang, B.; Liu, H.; Yao, J. Facile synthesis and characterization of graphene nanosheets. *J. Phys. Chem. C* **2008**, *112* (22), 8192–8195.
- (26) Jung, H. G.; Myung, S. T.; Yoon, C. S.; Son, S. B.; Oh, K. H.; Amine, K.; Scrosati, B.; Sun, Y. K. Microscale spherical carbon-coated Li₄Ti₅O₁₂ as ultra high power anode material for lithium batteries. *Energy Environ. Sci.* **2011**, *4* (4), 1345–1351.
- (27) Lowell, S.; Shields, J. E. *Powder Surf. Area Porosity* **1998**.
- (28) de Boer, J. A. *Struct. Prop. Porous Mater.* **1958**.
- (29) Banhart, F.; Ajayan, P. M. Carbon onions as nanoscopic pressure cells for diamond formation. *Nature* **1996**, *382* (6590), 433–435.
- (30) Murafa, N.; Stengl, V.; Houskova, V. Monodispersed spindle-like particles of titania. *Microsc. Microanal.* **2009**, *15* (Suppl. 2), 1036–1037.
- (31) Ping, X.; Zheng, S. B.; You, J. L.; Jiang, G. C.; Chen, H.; Zeng, H. Structure and raman spectra of titanium oxides. *Spectrosc. Spectral Anal. (Beijing, China)* **2007**, *27* (5), 936–939.
- (32) Kelly, S.; Pollak, F. H.; Tomkiewicz, M. Raman spectroscopy as a morphological probe for TiO₂ aerogels. *J. Phys. Chem. B* **1997**, *101* (14), 2730–2734.
- (33) Shao, G. S.; Zhang, X. J.; Yuan, Z. Y. Preparation and photocatalytic activity of hierarchically mesoporous-macroporous TiO_{2-xNx}. *Appl. Catal., B* **2008**, *82* (3–4), 208–218.
- (34) Bentley, F. F.; Smithson, L. D.; Rozek, A. L. *Infrared Spektra and Characteristic Frequencies 700–300 cm⁻¹*; Wiley-Interscience: New York, 1968.
- (35) Jere, G. V.; Patel, C. C. Infrared absorption studies on peroxy titanium sulphate. *Can. J. Chem.—Rev. Can. Chim.* **1962**, *40* (8), 1576.
- (36) Christy, A. A.; Kvalheim, O. M.; Velapoldi, R. A. Quantitative-analysis in diffuse-reflectance spectrometry - a modified Kubelka-Munk equation. *Vibr. Spectrosc.* **1995**, *9* (1), 19–27.
- (37) Reyes-Coronado, D.; Rodriguez-Gattorno, G.; Espinosa-Pesqueira, M. E.; Cab, C.; de Coss, R.; Oskam, G. Phase-pure TiO₂ nanoparticles: anatase, brookite and rutile. *Nanotechnology* **2008**, *19*, 14.
- (38) Serpone, N.; Lawless, D.; Khairutdinov, R. Size effects on the photophysical properties of colloidal anatase TiO₂ particles - size quantization or direct transitions in this indirect semiconductor. *J. Phys. Chem.* **1995**, *99* (45), 16646–16654.
- (39) Bhatkhande, D. S.; Pangarkar, V. G.; Beenackers, A. Photocatalytic degradation for environmental applications - a review. *J. Chem. Technol. Biotechnol.* **2002**, *77* (1), 102–116.
- (40) Lorences, M. J.; Patience, G. S.; Diez, F. V.; Coca, J. Transient n-butane partial oxidation kinetics over VPO. *Appl. Catal., A* **2004**, *263* (2), 193–202.
- (41) Djeghri, N.; Formenti, M.; Juillet, F.; Teichner, S. J. Photo-interaction on surface of titanium-dioxide between oxygen and alkanes. *Faraday Discuss.* **1974**, *58*, 185–193.
- (42) Wu, X. H.; Su, P. B.; Liu, H. L.; Qi, L. L. Photocatalytic degradation of Rhodamine B under visible light with Nd-doped titanium dioxide films. *J. Rare Earths* **2009**, *27* (5), 739–743.
- (43) Sasirekha, N.; Basha, S. J. S.; Shanthi, K. Photocatalytic performance of Ru doped anatase mounted on silica for reduction of carbon dioxide. *Appl. Catal., B* **2006**, *62* (1–2), 169–180.
- (44) Woan, K.; Pyrgiotakis, G.; Sigmund, W. Photocatalytic Carbon-Nanotube-TiO₂ Composites. *Adv. Mater.* **2009**, *21* (21), 2233–2239.